(c 1.7, dioxane), and 160 mg (75%) of (Z)-2-benzyl-3-(4-methoxybenzoyl)propenoic acid (IV) as the only detectable products. Compound (+)-I has NMR, IR, mass spectrum, and chromatographic behavior identical with that of (±)-I. Compound IV has different spectral and chromatographic behavior than (E)-2-benzyl-3-(4-methoxybenzoyl)propenoic acid (VII). $^1$H NMR ($CDCl_3$): δ 3.72 (br s, 2 H), 3.81 (s, 3 H), 6.71 (s, 1 H), 6.87 (d, J = 8.9 Hz, 2 H), 7.22–7.32 (m, 5 H), 7.64 (br, 2 H). IR ($CHCl_3$): 3420 m, 1772 s, 1725 m, 1600 s cm$^{-1}$. Mass spectrum: $M^+/e$ 296 (molecular ion), 278, 251, 161, 135, 107, 91, 77.

**CPA-Catalyzed Elimination Using 2-Benzyl-2-chloro-3-benzoylpropionic Acid (II) as the Sustrate.** By use of a procedure similar to that for (±)-I for the CPA-catalyzed elimination of HCl from (±)-II, compound (+)-II $[\alpha]^{25}_D$ = 62.0 (c 1.4, chloroform) and (Z)-2-benzyl-3-benzoylpropenoic acid (V) were isolated in over 70% yield by using 88% hexane, 10% ethyl acetate, and 2% acetic acid to elute the products from the silica column. No other product was detected. Compound (+)-II has NMR, IR, mass spectrum, and chromatographic behavior identical with that of (±)-II. Compound V has different NMR, IR, and chromatographic behavior than (E)-2-benzyl-3-benzoylpropenoic acid (VIII). $^1$H NMR ($CDCl_3$): δ 3.57 (s, 2 H), 6.70 (s, 1 H), 7.13–7.35 (m, 8 H), 7.46 (d, J = 6.0 Hz, 2 H). Mass spectrum: $M^+/e$ 266 (molecular ion), 248, 221, 105, 91, 77. IR ($CHCl_3$): 3565 m, 3280 m, br, 1765 s, 1600 m cm$^{-1}$.

**Deuteration of Alkenes. (a) Deuteration Employing Diimide.** Deuteration using reduction with diimide was carried out as described by Hamersma and Snyder.[26] In a typical deuteration experiment, a solution of 60 mg (0.2 mmol) of VII and 838 mg (4.3 mmol) of dipotassium azodicarboxylate was prepared in 4 mL of methyl alcohol-*d* under nitrogen. To the reaction mixture was added 145 μL (7.96 mmol) of deuterium oxide (or acetic acid-*d* for the reduction of V) in portions over 2–3 h and the resultant mixture allowed to stand for another 1 h. Then, the reaction was quenched with 10 mL of water and extracted with ethyl acetate. The ethyl acetate solution was washed with 2 M HCl followed by saturated NaCl and dried over $MgSO_4$. After solvent was evaporated under reduced pressure at ambient temperature, the residue was chromatographed on a silica column with a mixture of 76% hexane, 20% ethyl acetate, and 4% acetic acid to elute first the starting material, followed by the product.

**(b) Catalytic Reduction.** Compounds IV, V, VII, and VIII were reduced by deuterium gas in benzene by using palladium on carbon as the catalyst. In a typical reduction, 123 mg (46 mmol) of the alkene in 100 mL of benzene was treated with deuterium gas in the presence of 50 mg of 5% palladium on carbon for 90 min. Then, the catalyst was removed by filtration, and the solvent was evaporated under vacuum at ambient temperature. The residue was crystallized from chloroform and petroleum ether to yield 98 mg (71% yield) of product. The product of the reduction was chromatographically indistinguishable from 2-benzyl-3-(4-methoxybenzoyl)propionic acid (IX) when IV and VII were reduced and from 2-benzyl-3-benzoylpropionic acid (X) when V and VIII were reduced.

**Acknowledgment.** This research was supported in part by NIH Grant AM 32539. We appreciate helpful discussions with Dr, H. N. Bramson and aid in the experimental work by Dr. Thomas Spratt.

(26) Hamersma, J. W.; Snyder, E. J. *J. Org. Chem.* **1965**, *30*, 3985.

# Molecular Structure and Dynamics of Crystalline *p*-Fluoro-D,L-phenylalanine. A Combined X-ray/NMR Investigation

**Yukio Hiyama,[†] James V. Silverton,[‡] Dennis A. Torchia,*[†] J. T. Gerig,[§] and S. J. Hammond[§]**

*Contribution from the Mineralized Tissue Research Branch, National Institute of Dental Research, Laboratory of Chemistry, National Heart, Lung, and Blood Institute, National Institutes of Health, Bethesda, Maryland 20205, and Department of Chemistry, University of California, Santa Barbara, California 93106.* *Received June 28, 1985*

**Abstract:** We report the molecular structure and phenyl-ring dynamics of crystalline *p*-fluoro-D,L-[2,3,5,6-$^2H_4$]phenylalanine. Crystals of this molecule have space group $P\bar{1}$ and unit cell dimensions $a$ = 5.1927 (6) Å, $b$ = 5.4246 (4) Å, $c$ = 16.1318 (15) Å, $\alpha$ = 96.752 (8)°, $\beta$ = 94.060 (7)°, and $\gamma$ = 110.153 (7)°. In the crystals the molecules pack so that layers of strongly hydrogen-bonded atoms alternate with layers composed of the nonpolar phenyl rings. Phenyl-ring dynamics in the crystalline state was studied by $^2$H and $^{19}$F nuclear magnetic resonance (NMR) spectroscopy. Analysis of NMR line shapes and spin-lattice relaxation times ($T_1$) showed that the phenyl ring exhibited two types of motion: (a) a rapid, small-amplitude rolling motion about the Cβ–C1 bond axis and (b) a slower 180° flip about the Cβ–C1 axis. The rms amplitude of the rolling motion increased from less than 5° at 22 °C to 17° at 143 °C. At 143 °C the correlation time for the motion was less than $10^{-11}$ s. The correlation time for the 180° ring flip decreased from ca. $10^{-4}$ s at 22 °C to 4.8 × $10^{-8}$ s at 160 °C. The temperature dependence of the correlation time in the 100–160 °C temperature range was fit by using a simple activation equation that yielded an apparent activation energy of 47 kJ/mol and a preexponential factor of 4 × $10^{-14}$ s for the phenyl-ring flip process. $^2$H and $^{19}$F spectra of twinned crystals were used to determine the approximate orientation of the $^{19}$F chemical shift tensor. The most shielded tensor component was found to be normal to the phenyl ring while the intermediate shielded component was parallel to the C4–F bond axis.

Over the past decade various investigators have used nuclear magnetic resonance (NMR)[1] spectroscopy to study the motions of aromatic rings in amino acids, peptides, proteins, and synthetic polymers.[2-8] These studies have shown that, in addition to rapid, small-amplitude fluctuations, aromatic rings undergo 180° flips. The rates of ring flipping and the apparent activation energies

[†] National Institute of Dental Research.
[‡] National Heart, Lung, and Blood Institute.
[§] University of California.

(1) Abbreviations used: NMR, nuclear magnetic resonance; PFF, *p*-fluoro-D,L-phenylalanine; $d_4$PFF, *p*-fluoro-D,L-[2,3,5,6-$^2H_4$]phenylalanine; $d_7$PFF, *p*-fluoro-D,L-[2,3,5,6,*N*,*N*,*N*-$^2H_7$]phenylalanine; $d_3$PFF, *p*-fluoro-D,L-[*N*,*N*,*N*-$^2H_3$]phenylalanine; EFG, electric field gradient; $T_1$, spin-lattice relaxation time; $T_2$, transverse relaxation time; UV, ultraviolet spectroscopy.

0002-7863/86/1508-2715$01.50/0 

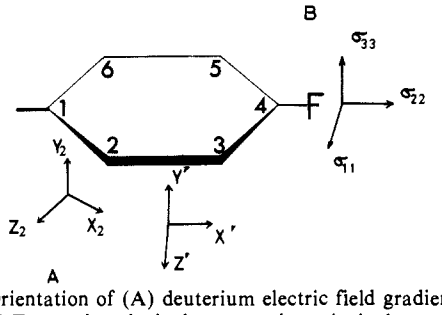


**Figure 1.** Orientation of (A) deuterium electric field gradient (EFG) tensor ($X_i$,$Y_i$,$Z_i$: static principal axes; major principal component $Z_i$ along $C_i$–$^2$H bond. $X'$,$Y'$,$Z'$: 180° ring flipping) and (B) fluorine chemical shift tensor $\sigma$ in fluorophenyl ring. Definition of the EFG axes: $|ZZ| \geq |YY| \geq |XX|$.

of the flip process vary greatly and are sensitive to the local environment of the ring. Indeed, the motivation behind many of these studies has been to probe the environments of the aromatic rings through a study of ring mobility.

Because of the connection between aromatic ring mobility and local structure, we decided to use solid-state NMR spectroscopy[9-11] to study phenyl-ring dynamics in a molecule having a defined crystal structure. The amino acid *p*-fluoro-D,L-phenylalanine (PFF) was well suited for this purpose since the molecule formed single crystals suitable for X-ray diffraction work. In addition, $^2$H and $^{19}$F NMR spectra of the amino acid deuterated at the 2, 3, 5, and 6 ring carbons ($d_4$PFF) showed that the phenyl ring was flexible on the NMR time scale in a convenient temperature range for NMR measurements of line shapes and spin–lattice relaxation times, $T_1$. Various papers describe how these parameters can be analyzed to obtain information about dynamics of solids.[10,11]

The study of molecular dynamics is simplified in the case of $^2$H because the major principal axis ($Z$) of the electric field gradient (EFG) tensor[12-15] $q_{ij}$ of deuterium is along the carbon–hydrogen bond[16-21] (Figure 1). The size of the nuclear quadrupole interaction, expressed in terms of the nuclear quadrupole coupling constant ($e^2Qq_{zz}/h$), falls in the range from 155 to 190 kHz with a small asymmetry parameter: $\eta$ [$=(q_{xx} - q_{yy})/q_{zz}$, $|q_{zz}| \geq |q_{yy}| \geq |q_{xx}|$] $\leq 0.1$.

A related goal of this work was to study phenyl-ring dynamics by using $^{19}$F. However, in contrast with the deuterium EFG, the orientation of the $^{19}$F chemical shift tensor in PFF was not known. We therefore determined the orientation of the $^{19}$F chemical shift tensor in crystalline PFF. The PFF molecule is a useful probe of phenyl-ring dynamics in proteins,[22] and information about the elements of the $^{19}$F chemical shift tensor will permit quantitative analysis of NMR parameters of this probe.

The outline of this paper is as follows. The crystal structure of PFF is described; then, the $^2$H line shapes and relaxation times of $d_4$PFF are presented and analyzed. Powder $^{19}$F line shapes and $T_1$ values are presented and are analyzed after the orientation of the $^{19}$F shift tensor is determined from $^2$H and $^{19}$F spectra on twinned crystals of $d_4$PFF. The paper concludes with a discussion of the relationship between the structural and dynamic features of the phenyl rings in crystalline PFF and with a comparison of phenyl-ring dynamics in PFF, L-phenylalanine hydrochloride (FHCL), and L-phenylalanine.

## Experimental Section

*p*-Fluoro-D,L-phenylalanine (PFF) was purchased from Calbiochem-Behring La Jolla, CA, and was used for NMR without further purification.

**Synthesis of *p*-Fluoro-D,L-[2,3,5,6-$^2H_4$]phenylalanine.** *p*-Fluoro-D,L-phenylalanine (Aldrich, 500 mg) was dissolved in $D_2O$ by addition of a few drops of NaOD solution, reprecipitated by the addition of $D_2SO_4$, and collected by filtration. To exchange the aromatic protons, this material was dissolved in a mixture of 3.5 g of $D_2SO_4$ and 0.5 g of $D_2O$ and heated in a 25-mL round-bottom flask under a nitrogen atmosphere at 140 °C in an oil bath. Loss of protons from the amino acid was followed by proton NMR spectroscopy; after 6 h the intensity of the aromatic signals had decreased to about one-third the intensity of the signals from the methylene group and did not appear to change further upon continued heating. The reaction mixture was poured onto 2.5 g of ice, and ammonium hydroxide was added carefully until the amino acid precipitated. The solid was collected by filtration and crystallized from $D_2O$ by adding, in turn, NaOD and $D_2SO_4$ to afford 180 mg of product. This was redissolved in 1.5 g of the $D_2SO_4/D_2O$ mixture and the resultant mixture heated at 140 °C for 5 h, followed by isolation and recrystallization as described for the first exchange. The proton NMR spectrum of the product, taken with a solution of the amino acid in $D_2O$/NaOD, showed a multiplet at $\delta$ 3.6 ppm ($-CH_2$), relative area 2, a multiplet at $\delta$ 4.2 (–CH), area 0.6, a doublet ($J$ = 9 Hz) at $\delta$ 7.8 (aromatic protons 3 and 5), area 0.1, and a doublet ($J$ = 6 Hz) at $\delta$ 7.95 (aromatic protons 2 and 6), area 0.15. UV analysis of the material indicated that it was essentially salt free.

It was observed that exchange of the aromatic protons under milder conditions (87% $D_2SO_4$ in $D_2O$ at 65 °C for 38 h) produced the 3,5-dideuterated amino acid.

**Crystal Growth.** Crystals of PFF were grown by slow cooling or evaporation from aqueous solution. Although the crystals obtained in this manner were twinned, a small single crystal, suitable for X-ray diffraction work, was obtained by dissecting a twinned crystal under a microscope. A much larger crystal, minimum weight ca. 50 $\mu$g, was required for $^{19}$F NMR work, and we were not successful in obtaining a single crystal of this size. The smallest crystal that we were able to use for NMR work had approximate dimensions 0.7 × 0.5 × 0.1 mm. We were unable to determine the unit cell parameters of this sample using X-ray diffraction techniques, and two $^{19}$F signals were observed in the NMR spectrum. These results are strong evidence that the crystal was twinned. The typical crystals used for NMR work weighed ca. 0.1 mg and were twinned.

**X-ray Diffraction.** The X-ray intensity data were collected at 22 (±1) °C with an Enraf-Nonius CAD4 diffractometer and Cu K$\alpha$ radiation ($\lambda$ = 1.5418 Å). Standard methods involving a prescan and maximum times of 120 s were employed to obtain 1715 intensities [460 with $I < \sigma(I)$]. There was no indication of radiation damage during data collection.

**NMR.** The 470.5-MHz fluorine-19 and 76.6-MHz deuterium spectra were taken by a Nicolet NIC-500 spectrometer with a 2090 Explorer digitizer and homemade probes. The fluorine probe contained a 4- or 5-mm i.d. solenoid coil, two Johansen capacitors, and a glass Dewar. There were two high-voltage Polyflon capacitors, a 5-mm, i.d. solenoid coil, and a glass Dewar in the deuterium probe. The "predelay" circuit in the NIC-500 was bypassed, and the spectrometer was used in the appropriate configuration. The deuterium NMR spectra at 38.45 MHz were obtained by a home-built spectrometer described elsewhere.[23] The

(2) Gall, C. M.; DiVerdi, J. A.; Opella, S. J. *J. Am. Chem. Soc.* **1981**, *103*, 5039.
(3) Rice, D. M.; Wittebort, R. J.; Griffin, R. G.; Meirovitch, E.; Stimson, E. R.; Meinwald, Y. C.; Freed, J. H.; Scheraga, H. A. *J. Am. Chem. Soc.* **1981**, *103*, 7707.
(4) Kinsey, R. A.; Kintanar, A.; Oldfield, E. *J. Biol. Chem.* **1981**, *256*, 9028.
(5) Torchia, D. A. *Annu. Rev. Biophys. Bioeng.* **1984**, *13*, 125.
(6) Wagner, G. *Q. Rev. Biophys.* **1983**, *16*, 1.
(7) Spiess, H. W. *Colloid Polym. Sci.* **1983**, *261*, 193.
(8) Cholli, A. L.; Dumais, J. J.; Engel, A. K.; Jelinski, L. W. *Macromolecules* **1984**, *17*, 2399.
(9) Haeberlen, U. *Advances in Magnetic Resonance*, Suppl. 1; Academic: New York, 1976.
(10) Speiss, H. W. *NMR Basic Princ. Prog.* **1978**, *15*.
(11) Mehring, M. *NMR Basic Princ. Prog.* **1983**, *11*.
(12) Das, T. P.; Hahn, E. L. *Nuclear Quadrupole Resonance Spectroscopy, Solid State Physics, Suppl.* 1; Seitz, F., Turnbull, D., Eds.; Academic: New York, 1958.
(13) Lucken, E. A. C. *Nuclear Quadrupole Coupling Constants*; Academic: New York, 1969.
(14) Abragam, A. *The Principles of Nuclear Magnetism*; Oxford: London, 1961.
(15) Slichter, C. P. *Principles of Magnetic Resonance*; Springer-Verlag: Berlin, 1978.
(16) Ellis, D. L.; Bjorkstaim, J. L. *J. Chem. Phys.* **1967**, *46*, 4660.
(17) Adriaenssens, G. J.; Bjorkstam, J. L. *J. Chem. Phys.* **1972**, *56*, 1223.
(18) Soda, G.; Chiba, T. *J. Phys. Soc. Jpn.* **1969**, *26*, 249.
(19) Da Graca, M.; Dillon, C.; Smith, J. A. S. *J. Chem. Soc., Faraday Trans. 2* **1972**, *68*, 2183.
(20) Achlama, A. M.; Zun, Y. *J. Magn. Reson.* **1979**, *36*, 249.
(21) Brown, T. L.; Butler, L. G.; Curtin, D. Y.; Hiyama, Y.; Paul, I. C.; Wilson, R. B. *J. Am. Chem. Soc.* **1982**, *104*, 1172.
(22) Gerig, J. T.; Hammond, S. J. *J. Am. Chem. Soc.*, **1984**, *106*, 8244.
(23) Sarkar, S. K.; Sullivan, C. E.; Torchia, D. A. *J. Biol. Chem.* **1983**, *258*, 9762.

Table I. Parameters for the Heavier Atoms[a]

| atom | x | y | z | U (e) |
|---|---|---|---|---|
| C | 6249 (5) | 1085 (5) | 5967 (2) | 263 (8) |
| O1 | 3955 (4) | 1355 (4) | 5957 (1) | 363 (7) |
| O2 | 8456 (4) | 2794 (3) | 5826 (1) | 369 (8) |
| Cα | 6442 (6) | −1549 (5) | 6164 (2) | 289 (9) |
| Cβ | 7743 (8) | −1328 (7) | 7058 (2) | 496 (11) |
| C1 | 6263 (7) | −507 (7) | 7746 (2) | 488 (11) |
| C2 | 7200 (15) | 2004 (9) | 8170 (4) | 980 (25) |
| C3 | 5979 (17) | 2804 (10) | 8825 (4) | 1120 (27) |
| C4 | 3755 (9) | 1050 (11) | 9056 (2) | 713 (17) |
| C5 | 2682 (10) | −1429 (15) | 8649 (4) | 879 (23) |
| C6 | 3933 (9) | −2191 (12) | 7988 (3) | 764 (19) |
| F | 2543 (6) | 1806 (7) | 9706 (2) | 1045 (14) |
| N | 8233 (5) | −2362 (4) | 5592 (2) | 301 (8) |

[a] Positional parameters are multiplied by 10000 and equivalent $U$ values by 10000. The equivalent $U$ values are the geometric means of the diagonal terms of the vibration tensors. In every case the anisotropic temperature factor had the form $\exp(-2\pi^2\sum_{ij}U_{ij}h_ih_ja_i^*a_j^*)$.

94-MHz fluorine spectra were recorded by the 500-MHz spectrometer console with a 2.3-T magnet. The 90° pulse was 2.2–2.5 μs for $^2$H and 3 μs for fluorine. In order to eliminate echo distortions caused by the large $^{19}$F chemical shift anisotropy, a Hahn echo sequence with EXORCYCLE phase cycling was employed for the fluorine NMR measurements.[24,25] The deuterium NMR spectra were obtained with a quadrupole echo pulse sequence[26-28] with a proper transmitter phase cycling to observe reliable line shapes. Delay times between the two pulses of the echo sequences were typically 10 and 30 μs for $^{19}$F and $^2$H, respectively. The free induction decay signals were left shifted until the echo maximum occurred at the first point in the time domain. Typical sampling rates were 1 MHz for $^{19}$F and 2 MHz for $^2$H NMR experiments. Spin–lattice relaxation times were measured by an inversion–recovery pulse sequence containing a 180° pulse, followed by the proper echo sequence for each nucleus.

## Results

**X-ray Crystal Structure.** Crystals of PFF are tabular, triclinic prisms with a tendency of twin parallel to the plate. It is possible to dissect out single crystals suitable for X-ray diffraction, and the following cell dimensions result: $a$ = 5.1927 (6), $b$ = 5.4246 (4), $c$ = 16.1318 (15) Å; $\alpha$ = 96.752 (8), $\beta$ = 94.060 (7), $\gamma$ = 110.153 (7)°. The space group is $P\bar{1}$.

The phase problem was solved with the programs of MULTAN78,[29] and all heavier atoms were visible in the best $E$ map although the details of the phenyl ring were somewhat nebulous. Standard refinement techniques, using the programs of XRAY72,[30] allowed assignment of atomic labels unequivocally, and all expected deuterium atoms were found. As expected, the molecule is a zwitterion with three deuterium atoms attached to the nitrogen atom. The final $R$ factor, with anisotropic thermal parameters used for the heavier atoms, was a little disappointing (0.0696), but the thermal parameters of the 2, 3, 5, and 6 carbon atoms of the phenyl ring are so large as to indicate a probable failure of the usual harmonic approximation to thermal motion. The thermal parameters of the deuterium atoms attached to the aforementioned carbon atoms are also very large, but there were no difficulties in achieving convergence in the least-squares refinement.

The final atomic parameters are given in Table I, and a listing of observed and calculated structure factors is available. The molecular dimensions are shown in Figure 2 and appear entirely consistent with those expected for an amino acid. The figure, in the absence of Greek letters in the ORTEP[31] font, has Cα and Cβ labeled as CA and CB, respectively. The Cα–N bond is longer than the 1.47 Å usual for an un-ionized N atom, and this is in accord with the zwitterionic structure. The acid C–O bonds are not significantly different in length, and the phenyl ring possesses no significant deviation from a 2-fold axis through C1 and F. The actual details of the different bond lengths in the ring are probably somewhat obscured by the high thermal motion, but the trends are as expected for the effect of the *p*-fluoro substitution. While the phenyl ring does deviate significantly from planarity, the actual distances from the least-squares plane are no greater than 0.02 Å.

All three deuterium atoms attached to the nitrogen atom are involved in hydrogen bonds. The distances N···O(1), N···O(2),

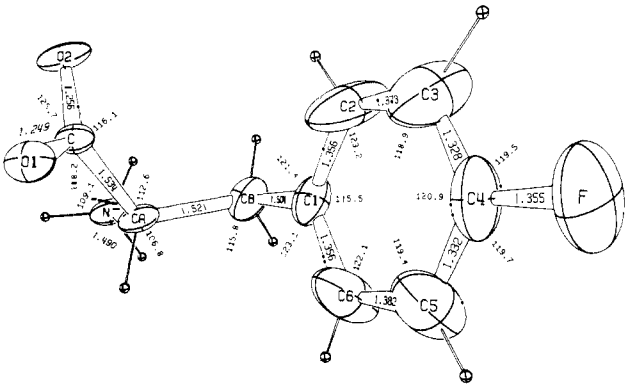


**Figure 2.** Molecular structure of *p*-fluoro-D,L-phenylalanine ($d_7$PFF) by X-ray diffraction.

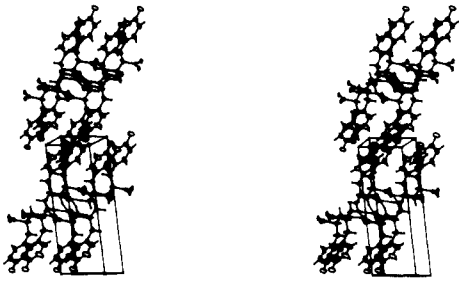

**Figure 3.** Stereoscopic view showing the packing of the *p*-fluoro-D,L-phenylalanine molecules in the unit cell. Note the bilayer structure of which a hydrophobic layer of phenyl rings alternates with a layer composed of hydrogen-bonded polar backbone atoms.

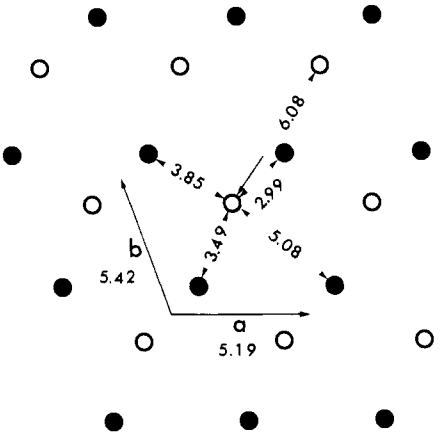


**Figure 4.** View (looking down the *c* axis of the unit cell) of fluorine atoms in two *ab* planes separated by 0.935 Å (●, $^{19}$F atom in lower plane; ○, $^{19}$F atom in upper plane) in the hydrophobic layer of the crystal. Interatomic distances are in Å.

(24) Bodenhausen, G.; Freeman, R.; Turner, D. L. *J. Magn. Reson.* **1977**, *27*, 511.
(25) Rance, M.; Byrd, R. A. *J. Magn. Reson.* **1983**, *52*, 221.
(26) Davis, J. H.; Jeffery, K. R.; Bloom, M.; Valic, M. I.; Higgs, T. P. *Chem. Phys. Lett.* **1976**, *42*, 390.
(27) Bloom, M.; Davis, J. H.; Valic, M. I. *Can. J. Phys.* **1980**, *58*, 1510.
(28) Speiss, H. W. *J. Chem. Phys.* **1980**, *72*, 6755.
(29) Main, P.; Hull, S. E.; Lessinger, L.; Germain, G.; Declercq, J. P.; Woolfson, M. M. MULTAN78, A System of Computer Programs for the Automatic Solution to Crystal Structures from X-ray Diffraction Data; Universities of York and Louvain: York, England, and Louvain, Belgium, 1978.
(30) Stewart, J. M.; Kruger, G. J.; Ammon, H. L.; Dickinson, C.; Hall, S. R. XRAY *System*, Version of Technical Report TR-192; University of Maryland: Baltimore, June 1972.
(31) Johnson, C. ORTEP, Report ORNL-3794; Oak Ridge National Laboratory: Oak Ridge, TN, 1965.

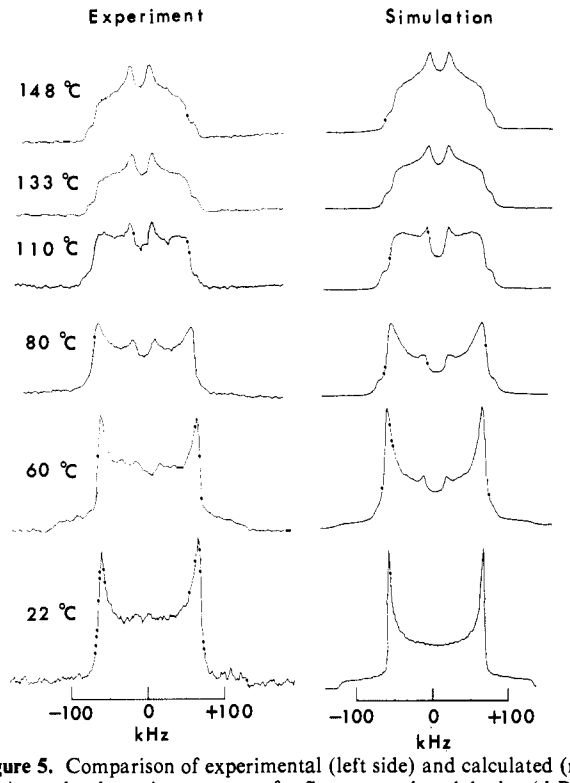


**Figure 5.** Comparison of experimental (left side) and calculated (right side) powder deuterium spectra of *p*-fluoro-D,L-phenylalanine ($d_4$PFF). Spectra were measured at 38.45 MHz by a quadrupole echo sequence with a 90° pulse of 2.3 μs. The spectra were calculated assuming 180° ring flips (correlation time $\tau$) with $\Theta$ = 59°, rapid rotations along the Cβ–Cl axis with an amplitude $\Phi_{rms}$, and static EFG parameters $\omega_Q/2\pi$ = 128 kHz ($e^2Qq_{zz}/h$ = 171 kHz, $\eta$ = 0). At 22 °C, $\tau = 10^{-4}$ s, $\Phi_{rms}$ = 0°; at 60 °C, $\tau = 1.6 \times 10^{-5}$ s, $\Phi_{rms}$ = 0°; at 80 °C, $\tau = 4 \times 10^{-6}$ s, $\Phi_{rms}$ = 6°; at 110 °C, $\tau = 3.2 \times 10^{-7}$ s, $\Phi_{rms}$ = 10°; at 133 °C, $\tau = 1.3 \times 10^{-7}$, $\Phi_{rms}$ = 13°; and at 148 °C, $\tau = 7.9 \times 10^{-8}$ s, $\Phi_{rms}$ = 15°. Extreme edges appear at $\pm 3e^2Qq_{zz}/4h$ (magnetic field $B_0$ is along with $Z$ axis), intermediate edges at $\mp 3e^2Qq_{zz}/8h(1 + \eta)$ ($=\pm 3e^2Qq_{yy}/4h$, $B_0$ along $Y$), and singularities at $\mp 3e^2Qq_{zz}/8h(1 - \eta)$ ($=\pm 3e^2Qq_{xx}/4h$, $B_0$ along $X$). $\Phi_{rms}$ was calculated from the observed reduction of width of powder pattern beyond that predicted by the 180° flip.

and N···O(1) are 2.930 (3), 2.738 (3), and 2.860 (3) Å, respectively, related by *a*, *b*, and the center of symmetry. The corresponding $^2$H···O distances are 2.03 (3), 1.67 (4), and 1.95 (4) Å with NH···O bond angles equal to 169°, 147°, and 142°. The packing is shown in Figures 3 and 4 and can be described as an infinite bilayer strongly held by hydrogen bonds in the *ab* plane with the hydrophobic phenyl rings on both sides of the layer. It is noteworthy that no carbon atom of the phenyl ring makes a contact as short as a van der Waals distance, although two fluorine atoms, related by the center of symmetry, are 2.990 (4) Å apart (approximately a van der Waals contact). The ready cleavage and slow growth in the *c* direction are thus consistent with the packing.

Since the two molecules in the unit cell are related by an inversion center, the $^{19}$F NMR spectrum of a single crystal will contain only one fluorine signal.

For comparison with crystalline PFF, crystals of D,L-phenylalanine were also prepared by slow cooling of an aqueous solution. The crystals appeared similar to those of the fluoro compound, but the tendency to twin was much more pronounced. In fact, all sizable crystals proved to be multiple twins, and the very few untwinned crystals were only a few microns thick. The thin crystals were very soft and tended to bend over a needle when attempts were made to isolate them. Several attempts were made to obtain single crystals by dissection of the thicker crystals, but without success. Characteristically, apparent cell dimensions were found that were different with different specimens, and the estimated standard deviations of the result were very poor. Such results probably indicate that no single crystal was ever obtained and the fairly good mechanical stability of large specimens was caused by the aggregation of many thin crystals. It is thus easy to understand the difficulties that must have been encountered in past attempts to obtain single crystals of phenylalanine of which no crystal structure has been reported. The X-ray powder data for D,L-phenylalanine[32] were indexed on a basis of the monoclinic space group $P2$ with cell dimensions $a$ = 12.93 Å, $b$ = 10.03 Å, $c$ = 6.428 Å, and $\gamma$ = 99.2°. The unit cell of the fluorine compound bears no obvious relationship to this. The addition of a fluorine atom must thus perturb the interatomic forces sufficiently so that crystal growth parallel to the plate (defined by *a* and *b*) is somewhat enhanced over that of the parent compound.

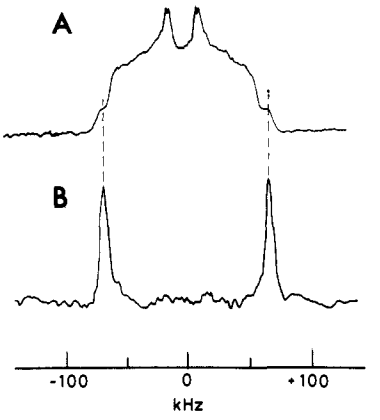


**Figure 6.** Comparison of twinned crystal and powder $^2$H quadrupole echo spectrum of *p*-fluoro-D,L-phenylalanine ($d_4$PFF) at 38.45 MHz and 143 °C. (A) Powder $^2$H spectra showing two sets of singularities with splitting of 27.5 and 22.0 kHz. (B) Twinned crystal $^2$H NMR spectrum at orientation $\theta$ = 90° and $\phi$ = 150° (see Figure 4).

**Table II.** Temperature and Field Dependence of $^2$H Spin–Lattice Relaxation Time of $d_4$PFF by Inversion Recovery[a]

| | $T_1$, ms | | | $T_1$, ms | |
|---|---|---|---|---|---|
| $T$, °C | at 38.45 MHz | at 76.76 MHz | $T$, °C | at 38.45 MHz | at 76.76 MHz |
| 22 | 60000[b] | | 110 | 200 | |
| 69 | 4700 | | 117 | 146 | |
| 80 | 2200 | | 121 | 104 | |
| 84 | | 5000 | 133 | 82 | |
| 90 | 790 | | 140 | 57 | |
| 98 | | 2200 | 148 | 47 | |
| 101 | 330 | | 160 | 32 | |

[a] Experimental error, ±10%. [b] Measured by 90°–t–90° method.

**Powder Deuterium NMR.** At 22 °C the deuterium powder spectrum of $d_4$PFF wax axially symmetric. The line shape changed dramatically with increasing temperature (Figure 5), and an axially asymmetric, $\eta \simeq 0.66$, spectrum was obtained at 148 °C. When the high-temperature spectrum was obtained with minimal filtering (Figure 6A), two maxima were observed at 27.5 and 22.0 kHz for each transition. This observation showed that the high-temperature spectrum was composed of two similar, but not identical, powder patterns.

Spin–lattice relaxation times were measured over a wide temperature range at 38.45 MHz. Since little $T_1$ anisotropy was observed in the experimental spectra, integrated signal intensities in inversion–recovery spectra were used to obtain average $T_1$ values, and the average $T_1$ values are tabulated in Table II along with average $T_1$ values measured at 76.76 MHz at two temperatures.

**Analysis of Powder Deuterium NMR Spectra.** The powder line shapes of $d_4$PFF, observed as a function of temperature, were simulated by using a two-site 180° ring-flip model (Figure 5, right side). Echo distortions resulting from finite pulse power[27] and short anisotropic $T_2$ values[32] were included in the line-shape calculations. In addition, distortion of the inversion-recovery $^2$H

(32) Khawas, B. *Acta Crystallogr., Sect. B: Struct. Crystallogr. Cryst. Chem.* **1971**, *B27*, 1517.
(33) Spiess, H. W.; Sillescu, H. *J. Magn. Reson.* **1981**, *42*, 381.

Table III. Temperature Dependence of the Correlation Time for the 180° Ring Flipping

| T, °C | correln time, s: from line-shape anal. | correln time, s: from $T_1$ measmnt[a] |
|---|---|---|
| 22 | $1.0 \times 10^{-4}$ (order of magnitude) | $9.2 \times 10^{-5}$ (±20%) |
| 60 | $1.6 \times 10^{-5}$ (+100%–50%) | |
| 69 | | $7.3 \times 10^{-6}$ |
| 80 | $4.0 \times 10^{-6}$ (±50%) | $3.4 \times 10^{-6}$ |
| 84 | | $2.1 \times 10^{-6}$ [b] |
| 90 | | $1.2 \times 10^{-6}$ |
| 98 | | $9.2 \times 10^{-7}$ [b] |
| 101 | | $5.1 \times 10^{-7}$ |
| 110 | $3.2 \times 10^{-7}$ (±20%) | $3.1 \times 10^{-7}$ |
| 117 | | $2.2 \times 10^{-7}$ |
| 121 | | $1.7 \times 10^{-7}$ |
| 133 | $1.3 \times 10^{-7}$ (±10%) | $1.2 \times 10^{-7}$ |
| 140 | | $8.7 \times 10^{-8}$ |
| 148 | $7.9 \times 10^{-8}$ (±20%) | $7.2 \times 10^{-8}$ |
| 160 | | $4.8 \times 10^{-8}$ |

[a] Uncertainity, ±10%. [b] At 76.76 MHz.

spectra due to a finite 180° pulse (intensity $\omega_1$) was included in the theoretical spectra by considering off-resonance, $\Delta\omega_Q$. Following Vega and Pines,[34] the longitudinal magnetization at the end of the 180° pulse, $I_z$, is given by eq 1 where $I_{z0}$ is $z$ magnetization before the 180° pulse and $R = \Delta\omega_Q/2\omega_1$.

$$I_z = I_{z0}\{\cos[(1 + R^2)^{1/2}\pi] \cos(R\pi) + [R/(1 + R^2)^{1/2}] \sin[(1 + R^2)^{1/2}\pi] \sin(R\pi)\} \quad (1)$$

The correlation times obtained from the simulations at various temperatures are listed in Table III. When the flip rate, $k$,[35] differs greatly from the quadrupole splitting, $\omega_Q$, the line shape is insensitive to the value of the correlation time, $\tau$, where $\tau = 1/(2k)$. For this reason, accurate correlation times could be obtained only over a narrow temperature range around 100 °C. Further, the best fits to the experimental line shapes were obtained only at temperatures above 100 °C. The larger uncertainties in the correlation times obtained at lower temperatures are a consequence of the poorer fits obtained in this temperature range. Therefore, no attempt was made to determine the activation energy for ring flips from the line-shape analysis.

The width of the powder pattern observed at 148 °C was 8% less than the width of the spectrum calculated with (a) 180° flips and (b) the static nuclear quadrupole parameters measured at 22 °C, $\omega_Q/2\pi = 128$ kHz [$(\omega_Q/2\pi = 3e^2Qq_{zz}/4h)$] and $\eta < 0.02$. This discrepancy in the width of the observed and calculated spectra is removed if one assumes that the $^2$H EFG is also averaged by rapid ($\tau \ll 10^{-8}$ s), small-amplitude (rms angle of 15°) reorientation about the Cβ–C1 bond axis. This motion together with 180° flips yields a calculated spectrum in agreement with the spectrum observed at 148 °C.

It was noted earlier that two maxima, separated by ca. 5 kHz, were observed in the high-temperature spectrum of $d_4$PFF. The ring-flip model readily accounts for this observation because the positions of the maxima of the averaged patterns are sensitive functions of the angles, Θ, made by the C–$^2$H bond axes and the ring flip axis, the Cβ–C1 bond axis. If the angle made by the C2–$^2$H bond axis with the flip axis differs by 1° from the angle made by the C3–$^2$H bond axis and the flip axis, the maxima of the powder patterns of deuterons at the 2 and 3 ring positions will differ by 6 kHz. (By symmetry, deuterons at ring positions 2 and 6 and at positions 3 and 5 give identical powder patterns.) The $^{19}$F–$^2$H dipolar splitting is negligible, less than 0.2 kHz, at this orientation. We therefore assign the splitting of the maxima in the high-temperature spectrum to a small difference (<1°) in angle made by the flip axis with the C–$^2$H bond axes ortho and meta to the fluorine atom.

The analysis of the $d_4$PFF powder line shape provided strong evidence that the phenyl ring flipped about the Cβ–C1 axis with

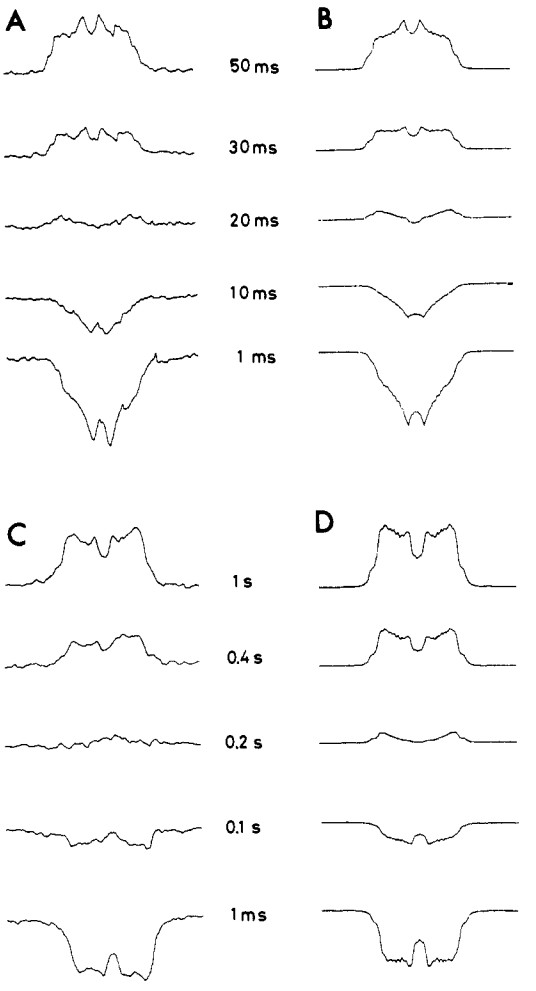


Figure 7. Experimental (A, +160 °C; C, +100 °C) and calculated (B, $\tau = 4.8 \times 10^{-8}$ s; D, $\tau = 6.1 \times 10^{-7}$ s) inversion–recovery spectra of $d_4$PFF. The 180° pulse was 4.6 μs. Delay time between the two 90° pulses was 30 μs.

correlation time that decreased from ca. $10^{-4}$ s at 22 °C to $8 \times 10^{-8}$ s at 148 °C. Analysis of $^2$H spin–lattice relaxation times strongly support the results of the line-shape analysis. The $^2$H spin–lattice relaxation time when the C–$^2$H bond axis undergoes a two-site flip[36] is given by eq 2 where Θ is the angle made by

$$1/T_1 = \tfrac{1}{8}\omega_Q^2 \sin^2(2\Theta)\{[\cos^2\theta + \cos^2(2\theta) - [0.75 \sin^2(2\theta) - \sin^4\theta]\cos(2\phi)]g(\omega_0,\tau) + [4 \sin^2\theta + \sin^2(2\theta) - 4 \sin^4\theta \cos(2\phi)]g(2\omega_0,\tau)\}$$

$$g(\omega_0,\tau) = \tau/(1 + \omega_0^2\tau^2) \quad (2)$$

the C–$^2$H bond axis and the flip axis, $(\theta,\phi)$ are the polar coordinates of the static field, $B_0$, $\omega_Q = 3e^2Qq_{zz}/4\hbar$, $\omega_0$ is the Larmor frequency, and $\tau$ is the correlation time. The line-shape analysis and the field dependence of the inversion–recovery spectra showed that the correlation times for the two-site flip motion satisfied the slow-motion condition $(\omega\tau)^2 \gg 1$ over the entire temperature range. In this limit the calculated inversion–recovery line shapes (Figure 7B,D) were slightly anisotropic and fitted well to the observed line shapes above 130 °C (e.g., Figure 7A). However, below 120 °C the observed inversion–recovery line shapes (e.g., Figure 7C) did not follow the theoretical prediction, showing nearly isotropic spin–lattice relaxation. This was presumably because spin diffusion[37] was enhanced by the large natural line widths (small $T_2$ values) that arise as a consequence of slow ring flips at the lower temperature. For this reason, average $T_1$ values were measured and were analyzed by using the expression for the

(34) Vega, S.; Pines, A. *J. Chem. Phys.* **1977**, *66*, 5624.
(35) $k$ is the same as Ω in ref 10 and 14 and as κ in ref 11.
(36) Torchia, D. A.; Szabo, A. *J. Magn. Reson.* **1982**, *49*, 107.
(37) VanderHart, D. L.; Garroway, A. N. *J. Chem. Phys.* **1979**, *71*, 2773.

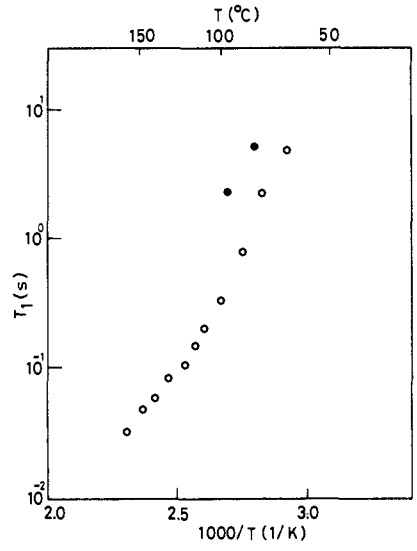


**Figure 8.** Temperature dependence of $^2H$ spin–lattice relaxation time in *p*-fluoro-D,L-phenylalanine ($d_4$PFF): O, 38.45 MHz; ●, 76.7 MHz.

average $T_1$ value, $\langle 1/T_1 \rangle$, obtained by averaging eq 2 over $(\theta,\phi)$ to give

$$\langle 1/T_1 \rangle = \tfrac{1}{5}(\omega_Q/\omega_0)^2\tau^{-1} \sin^2(2\Theta) \quad (3)$$

By use of the measured values of $\langle 1/T_1 \rangle$ (Table II), together with eq 3 with $\omega_Q/2\pi$ = 125 kHz, $\omega_0/2\pi$ = 38.45 MHz, and $\Theta$ = 60°, values of $\tau$ were calculated and plotted as a function of temperature (Figure 7). Following Andrew and colleagues,[38-40] we assumed that the correlation time for the phenyl-ring flips followed a simple activation law (eq 4) It was found that a single straight

$$\tau = \tau_0 \exp(E/kT) \quad (4)$$

line did not provide a good fit to the data in Figure 8; however, the points above 100 °C were well fit by a least-squares straight line having $E$ = 47 kJ/mol (11.3 kcal/mol) and $\tau_0 = 4 \times 10^{-14}$ s. In similar fashion the points obtained at temperatures below 100 °C were also well fit by a straight line having $E$ = 83 kJ/mol (20 kcal/mol) and $\tau_0 = 1.1 \times 10^{-18}$ s. Unlike the physically reasonable value of $\tau_0$ obtained from the fit to high-temperature data, the value of $\tau_0$ obtained from the low-temperature data is 4–5 orders of magnitude smaller than the correlation time calculated for a freely rotating phenyl ring. This problem does not arise if one assumes that $E$ decreases slightly between room temperature and 100 °C. For instance, if $E$ is reduced from 53 to 47 kJ/mol in this temperature range, eq 4 fits the observed points in Figure 8 quite well with $\tau_0 = 4 \times 10^{-14}$ s. Therefore, an activation energy of 47–53 kJ/mol (11–12 kcal/mol) with $\tau_0 = 4 \times 10^{-14}$ s is able to describe the temperature dependence of $\tau$ from 20 to 150 °C.

Although reorientation about the Cβ–C1 bond axis was neglected in the analysis of the PFF line shapes and $\langle 1/T_1 \rangle$ values, we calculated that this introduced an error of less than 15% in $\tau$, provided that the rolling motion was fast ($\tau_{roll} < 10^{-11}$ s) and had a small angular amplitude ($\Phi_{rms} < 20°$). The result that the correlation times for 180° ring flips obtained from the line shapes, agreed with those obtained from $T_1$ measurements (Table III) was further evidence that only minor errors in $\tau$ resulted from neglecting the rapid, small-amplitude rolling motion of the phenyl ring.

**Fluorine Powder NMR Spectra.** Spectra of $d_7$PFF (PFF deuterated at the four ring carbons and at the amine nitrogen)

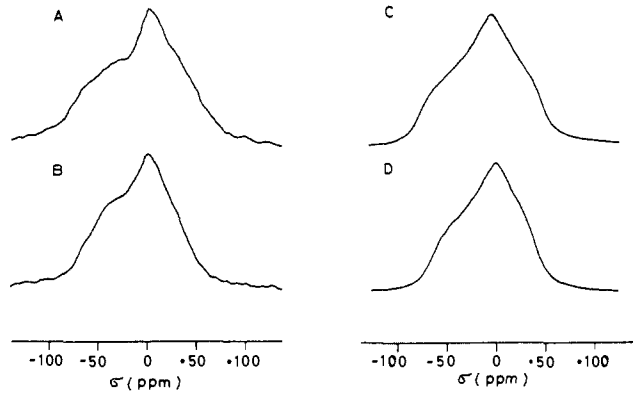


**Figure 9.** Comparison of 470-MHz experimental powder $^{19}F$ NMR spectra and calculated spectra of *p*-fluoro-D,L-phenylalanine ($d_7$PFF) at two temperatures: A, +22 °C; B, +143 °C; C, simulation of 22 °C spectrum, $\sigma_{11}$ = −75 ppm, $\sigma_{22}$ = 0 ppm, $\sigma_{33}$ = +50 ppm, 9-kHz Lorentzian broadening; D, simulation of 143 °C spectrum, $\sigma_{11}$ = −65 ppm, $\sigma_{22}$ = 0 ppm, $\sigma_{33}$ = +40 ppm, 9-kHz Lorentzian broadening. Experimental spectra obtained by using an EXORCYCLE pulse sequence with a 90° pulse of 3 μs. Chemical shift reference: external $CaF_2$. A singularity occurs at $\sigma_{22}$, and edges are observed at $\sigma_{11}$ and $\sigma_{33}$ corresponding to $B_0$ orientated along the principal values of the chemical shift tensor, $\sigma_{ii}$ ($\sigma_{11} < \sigma_{22} < \sigma_{33}$), in the $^{19}F$ NMR spectrum.

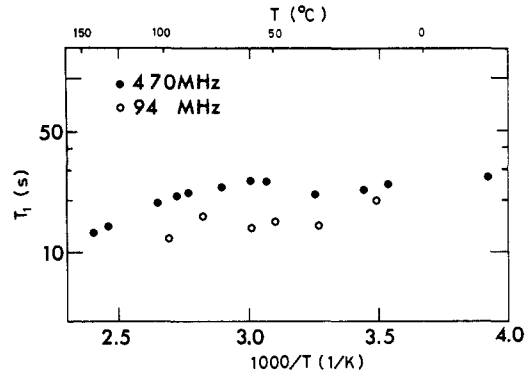


**Figure 10.** Temperature dependence of $^{19}F$ spin–lattice relaxation time ($T_1$) of *p*-fluoro-D,L-phenylalanine ($d_7$PFF) measured at two field strengths: O, 94 MHz; ●, 470 MHz.

at 22 and 143 °C (Figure 9) are axially asymmetric chemical shift powder patterns. Although proton–fluorine dipolar broadening was reduced by using the $d_7$PFF, fluorine–fluorine broadening remained, as expected from the crystal structure. At 22 °C the three principal elements of the fluorine chemical shift tensor, $\sigma_{11}$, $\sigma_{22}$, $\sigma_{33}$, were determined to be −75, 0, and +50 ppm, respectively (relative to $CaF_2$) by a computer simulation (Figure 9C). At 143 °C the simulation (Figure 9D) showed that $\sigma_{22}$ was equal to the value obtained at 22 °C but that $\sigma_{11}$ and $\sigma_{33}$ had moved closer to the isotropic chemical shift at the higher temperature. Consequently, the chemical shift anisotropy, $\sigma_{33} - \sigma_{11}$, decreased from 125 ppm at 22 °C to 105 ppm at 143 °C. No further increase in $\sigma_{33} - \sigma_{11}$ was observed when the temperature was lowered from room temperature to −80 °C.

The temperature dependence of the $^{19}F$ spin–lattice relaxation time of $d_7$PFF was measured at 94 and 470 MHz. At both field strengths, $T_1$ was nearly independent of temperature (Figure 10), and at 470 MHz, anisotropy in $T_1$ was not observed.

**Orientation of the Fluorine Chemical Shift Tensor: $^2H$ and $^{19}F$ NMR of a Twinned Crystal.** In order to analyze the $^{19}F$ powder line-shape and relaxation data, it was necessary to determine the orientation of the $^{19}F$ chemical shift tensor. Normally it is straightforward to determine the orientation of a chemical shift tensor when the crystal structure is known. However, all crystals of PFF that were large enough for NMR work were found to be twinned. A polarizing microscope showed that the crystals had the shape illustrated in Figure 11. The crystal-fixed $X,Y,Z$ coordinate system shown in Figure 11 was used to define the

(38) Andrew, E. R.; Hinshaw, W. S.; Hutchins, M. G.; Sjoblom, R. O. I. *Mol. Phys.* **1976**, *31*, 1479.
(39) Andrew, E. R.; Hinshaw, W. S.; Hutchins, M. G.; Sjoblom, R. O. I. *Mol. Phys.* **1976**, *32*, 795.
(40) Andrew, E. R.; Hinshaw, W. S.; Hutchins, M. G.; Sjoblom, R. O. I. *Mol. Phys.* **1977**, *34*, 1695.

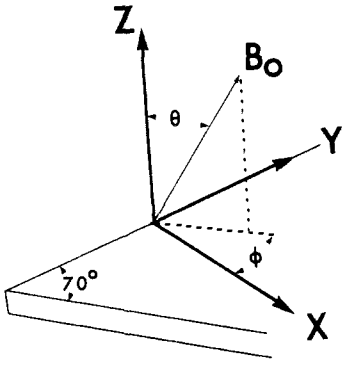


**Figure 11.** Morphology of the *p*-fluoro-D,L-phenylalanine crystal used for NMR work showing the orientation of the crystal coordinate system $(X,Y,Z)$. The polar angles $(\theta,\phi)$ define the orientation of $B_0$ in the $(X,Y,Z)$ system.

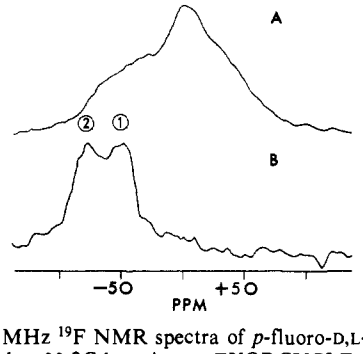


**Figure 12.** 470 MHz $^{19}F$ NMR spectra of *p*-fluoro-D,L-phenylalanine ($d_7$PFF) obtained at 22 °C by using an EXORCYCLE pulse sequence with 3-μs 90° pulse: (A) powder; (B) twinned crystal with orientation defined by $(\theta,\phi) = (90°, 150°)$.

orientation of the external field, $B_0$, relative to the crystal. The coordinate system was uniquely defined because the upper and lower surfaces of the $XY$ plane were easily distinguished. The $^{19}F$ spectrum shown in Figure 12 was obtained at 22 °C, and $B_0$ had orientation $(\theta,\phi) = (90°,150°)$. Because the crystal was twinned, two $^{19}F$ signals were observed in the spectrum and are designated F1 (at −50 ppm) and F2 (at −75 ppm). Note that the chemical shift of F2 is at the downfield edge ($\sigma_{11}$) of the $^{19}F$ powder pattern. This implies that the chemical shift tensor of the fluorophenyl ring corresponding to the F2 signal had $\sigma_{11}$ along $B_0$. In order to determine the orientation of $B_0$ relative to the fluorophenyl ring, a $^2H$ spectrum (Figure 6B) was obtained with $B_0$ in the same orientation (relative to the crystal axis system) that was used to obtain the $^{19}F$ spectrum. This spectrum was obtained at 143 °C where $T_1$ was small as a consequence of rapid ring flips. At room temperature, a $^2H$ spectrum was not observed because $T_1$ was too large. The $^2H$ spectrum of the orientated crystal shows a single doublet whose splitting, 136 kHz, is close to the splitting observed for the extreme edges [$B_0$ is along the major ($Z$) axis of the EFG] of the motionally averaged powder pattern (Figure 6A). As a consequence of two-site flips, the extreme edges of the averaged powder pattern correspond to $B_0$ orientated in the plane of the ring orthogonal to the C4–F bond axis and parallel to the C3–C5 internuclear vector (see $X',Y',Z'$ in Figure 1). This result, together with the assignment of $B_0$ along $\sigma_{11}$ from the $^{19}F$ spectrum, shows that $\sigma_{11}$ is in the plane of the ring, orthogonal to the C4–F bond and parallel to the C3–C5 axis.

One quesion regarding the $^2H$ spectrum that remains to be answered is where the doublet corresponding to the F1 phenyl ring in Figure 6B is. We think that this signal was not observed because the relative orientation of $B_0$ with respect to the F1 ring was such that $T_2$ was small. A small $T_2$ reduced the signal-to-noise ratio because the signal width was large and because signal intensity was irreversibly lost during the formation of the quadrupole echo.

Thus far, we have presented data obtained at one orientation of $B_0$ in the crystal-fixed frame (90°,150°). The positions of the two fluorine signals, measured as $\phi$ varied from 0 to 180° (with

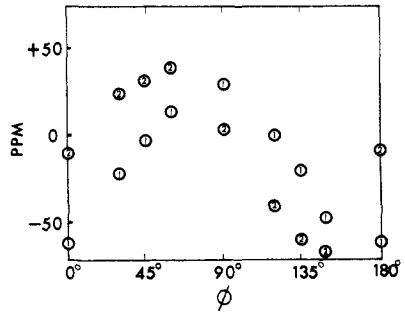


**Figure 13.** $^{19}F$ NMR rotation pattern of a twinned *p*-fluoro-D,L-phenylalanine ($d_7$PFF, $d_4$PFF) crystal obtained at 22 °C and 470 MHz. As the crystal was rotated, $\theta$ was fixed as 90° and $\phi$ was variable [see Figure 11 for definition of $(\theta,\phi)$].

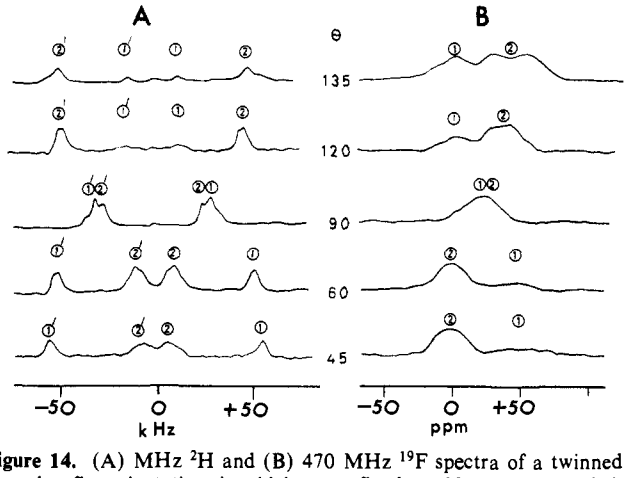


**Figure 14.** (A) MHz $^2H$ and (B) 470 MHz $^{19}F$ spectra of a twinned crystal at five orientations in which $\phi$ was fixed at 60° and $\theta$ was varied. Note that the two sites (1 and 2) in the twinned crystal are not equally populated.

$\theta = 90°$), showed the expected sinusoidal dependence upon $\phi$ (Figure 12). The separation of the signals was largest at $\phi = 0°$, attaining a value of ca. 30 kHz at 470 MHz. At 94 MHz, the signal separation (with $\theta = 90°$ and $\phi = 0°$) was 5 times smaller. The result confirmed the assignment of the two $^{19}F$ signals to two different orientations of the two $^{19}F$ sites in the twinned crystal. Spectra of several twinned crystals, each crystal oriented in the same way relative to $B_0$, were recorded, and the separation of the two $^{19}F$ signals was the same in each case. However, the relative intensities of the two signals varied from 1 to 1 to 3 to 1. As will be seen, the availability of crystals with fluorine signals having unequal intensities proved to be highly useful.

The rotation plot in Figure 13 together with the high-temperature $^2H$ data showed that $\sigma_{11}$ was along the C3–C5 internuclear vector. In order to determine the orientations of the other principal directions of the $^{19}F$ chemical shift tensor, the crystal was oriented so that $B_0$ was normal to the C3–C5 internuclear vector (i.e., $\phi = 60°$), and $^{19}F$ and $^2H$ spectra were measured as a function of $\theta$ (Figure 14).

In the particular crystal chosen for this part of the study the relative intensity of F2 and F1 in each fluorine spectrum was about 3 to 1. We were able to use the unequal relative intensities to assign the F1 and F2 sites in the $^2H$ spectra obtained as a function of $\theta$ (Figure 14). At $\theta = 135°$, the F2 fluorine signal (a broad doublet, to be discussed below) was observed as the most shielded position, 50 ppm, observed in the powder spectrum. The corresponding F2 deuterium resonance (at 143 °C) occurred at the intermediate edge of the averaged $^2H$ powder spectrum, showing that $B_0$ was normal to the phenyl ring (Figure 1). When the crystal orientation was changed by 90°, $\theta = 45°$, the F2 fluorine signal was observed at the $\sigma_{22}$ shielding position, 0 ppm, as expected. At this orientation, the F2 $^2H$ signals were observed at the positions of the singularities [$B_0$ is along the $X$ ($X'$ in Figure 1) axis of the $^2H$ EFG] of the high-temperature (averaged) $^2H$ powder pattern. This shows that, at this orientation, $B_0$ was

parallel to the C4–F bond axis.

From the rotation patterns (Figures 13 and 14), one can estimate the relative orientations of the two distinct sites in the twinned crystal. The C3–C5 axes in the two sites are nearly parallel, and the orientation of the two other principal axes in the second site is obtained by rotating these axes, in the first site, by 90° around the C3–C5 axis. this relation between the two sites can be obtained by a mirror operation in the crystal *ab* plane.

In closing this section, we note that the signal broadening observed in Figure 13, especially at $\theta = 135°$, was accounted for by $^{19}F$–$^{19}F$ dipolar coupling. The second moment of the $^{19}F$ signal was calculated assuming dipole–dipole coupling to the 10 nearest neighbors of the spin. The calculation showed that the value of the root-mean-square second moment was strongly anisotropic, changing from a minimum value of 1.5 kHz to a maximum value of 6.2 kHz as the orientation of $B_0$ relative to crystal fixed axes changed. The large anisotropy is a consequence of the two-dimensional layer arrangement of the $^{19}F$ nuclei in the crystal (Figures 3 and 4). The values of the calculated rms second moments are (a) 4.1 kHz, (b) 2.1 kHz, and (c) 4.1 kHz for the field direction perpendicular to (a) the phenyl ring, (b) the C4–F bond axis, and (c) the C3–C5 bond axis. These values of the rms second moment account for the line width observed in Figure 14.

We have utilized our knowledge of the deuterium EFG tensor orientation to determine the orientation of the fluorophenyl ring of PFF in the twinned crystal. In similar manner the $^{14}N$ EFG tensor orientation in *N*-acetylvaline[41] was determined by using the $^{14}N$–$^{1}H$ dipolar coupling tensor, and the phenyl-ring orientation in tetrafluoroterephthalic acid[42] was determined by using the $^{19}F$ chemical shift tensor.

In summary, we found the most shielded $\sigma_{33}$, direction of the fluorine chemical shift tensor to be normal to the phenyl ring. The direction of the intermediate shielding, $\sigma_{22}$, was along the C4–F bond axis. These results have an uncertainty of ±10° because of the width of the $^{19}F$ signals and errors in measuring the orientation of the crystal axis with respect to $B_0$. The $^{19}F$ chemical shift tensor found here in PFF is similar to that determined in 4,4′-difluorobiphenyl.[43]

**Analysis of Powder $^{19}F$ NMR Spectra.** The work with the twinned crystals showed that $\sigma_{22}$ was parallel to the C4–F bond axis and that $\sigma_{11}$ and $\sigma_{33}$ were orthogonal to this axis. This result showed why 180° flips of the phenyl ring did not affect the $^{19}F$ chemical shift tensor and explained why the width of the $^{19}F$ powder spectrum at 143 °C was nearly as large as the width of the spectrum at 22 °C. The reduced width observed at high temperature resulted from reductions in $|\sigma_{11}|$ and $|\sigma_{33}|$ whereas $\sigma_{22}$ remained constant. This observation showed that the motion responsible for the reduction in powder line width at high temperature did not involve fluctuations in the C4–F bond axis orientation. Therefore, the motion that averaged the $^{19}F$ powder spectrum at high temperature is a reorientation about the C4–F (or Cβ–C1) bond axis. By use of this model, the observed powder spectrum at 143° was simulated assuming a rolling motion, having an rms[23] angle, $\Phi_{rms}$ of 17°, about the Cβ–C1 bond axis. The absence of a discernible difference in the width of the powder spectra obtained at 22 and −90 °C showed that the angular fluctuation due to the rolling motion about the Cβ–C1 axis was less than 5° rms at 22 °C.

In order to analyze the $T_1$ data measured at 94 and 470 MHz (Figure 10), we consider two possible relaxation mechanisms: (a) chemical shift anisotropy and (b) $^{1}H$–$^{19}F$ dipole–dipole coupling. The latter mechanism is likely to be important at 94 MHz where $(\omega_I - \omega_S) \simeq 4 \times 10^7\ s^{-1}$ is within 1 order of magnitude of $\tau^{-1}$ for 180° ring flips at high temperature (Table III). In the case of a two-site flip, the orientation-dependent, $1/T_1$, and orientation-averaged, $\langle 1/T_1 \rangle$, dipolar relaxation rates[44] are given by eq 5 and eq 6, respectively. The observed $T_1$ values were not an-

$$1/T_1 = {}^9/_{16}\omega_D^2 \sin^2(2\Theta)\{\sin^4\theta(1 - \cos\phi)g(\omega_I - \omega_S,\tau) + 2[\sin^2\theta + \sin^2(2\theta)/4 + \sin^4\theta\cos\phi]g(\omega_I,\tau) + [1 + 6\cos^2\theta + \cos^4\theta - \sin^4\theta\cos(4\phi)]g(\omega_I + \omega_S,\tau)\} \quad (5)$$

$$\langle 1/T_1 \rangle = {}^3/_{10}\omega_D^2 \sin^2(2\Theta)\{g(\omega_I - \omega_S,\tau) + 3g(\omega_I,\tau) + 6g(\omega_I + \omega_S,\tau)\} \quad (6)$$

isotropic, so eq 6 was used to analyze the measure values of $1/T_1$. Applying eq 6 at 94 MHz and 110 °C, where $\tau = 3 \times 10^{-7}$ s for the ring flip and $\Theta = 53.8°$ from the X-ray structure, we calculate an average $T_1$ of 1 s using a $^{19}F$–$^{1}H$ internuclear distance of 2.55 Å [$\omega_D = \hbar\gamma_I\gamma_S/r^3$, $\omega_D/2\pi = 7.7$ kHz]. Only 10% of the $^{19}F$ nuclei have protons as nearest neighbors in the ring-deuterated PFF compounds studied. Therefore, the average $T_1$ of all the fluorine nuclei was calculated to be 10 s, assuming that $^{19}F$–$^{19}F$ spin diffusion distributed magnetization among all $^{19}F$ spins. This $T_1$ value is in good agreement with the value measured at 110 °C (Figure 10).

At 470 MHz, eq 5 predicts that the average $T_1$ will be 25 times longer than that observed at 94 MHz. Since this was clearly not the case (Figure 10), we considered that chemical shift anisotropy was the cause of spin–lattice relaxation at the high field. Because the 180° ring flips do not affect the chemical shift tensor (note that, by symmetry, this is true if the orientation of the CSA tensor differs from that shown in Figure 1), we calculated relaxation rates assuming that the shift anisotropy was modulated by a small-amplitude[44] rolling motion about the Cβ–C1 axis. Using the formalism of Torchia and Szabo,[36] we found that

$$1/T_1 = {}^9/_4(\sigma_{zz}\omega_0)^2\Phi_{rms}^2(1 + \eta/3)^2[\cos^2(2\theta)\cos^2\phi + \cos^2\theta\sin^2\phi]g(\omega,\tau) \quad (7)$$

and

$$\langle 1/T_1 \rangle = {}^9/_{10}(\sigma_{zz}\omega_0)^2\Phi_{rms}^2(1 + \eta/3)^2\tau \quad (8)$$

Since $T_1$ was not anisotropic, eq 8 was used to analyze the high-temperature $T_1$ measurements at 470 MHz. At 143 °C, the average $T_1$ value was measured as 13 s. At this temperature, $\Phi_{rms}$ was found to be 17° from the analysis of the powder line shape. The other parameters needed in eq 8, $\sigma_{zz}\omega_0$ and $\eta$,[45] were obtained from the simulation of the room-temperature powder pattern of $d_7$PFF. Inserting these measured parameters into eq 8 leads to the result that $\tau = 1.3 \times 10^{-11}$ s for the rolling motion at 143 °C. This value of the correlation is an upper bound since it was derived on the assumption that the measured relaxation rate $\langle 1/T_1 \rangle$ was due entirely to the chemical shift relaxation mechanism. Finally we note that the large anisotropy in $T_1$ predicted by eq 7 was not observed. The predicted anisotropy in $T_1$ remains large even if the orientation of the CSA tensor differs by 10° from that shown in Figure 1. Probably fluorine spin diffusion equalized the $T_1$ values for $^{19}F$ nuclei in all orientations.

Although the dipolar and chemical shift interactions were able to account for the average relaxation times measured at 94 and 470 MHz at high temperature, these interactions predict a large increase in average $T_1$ values as temperature decreases, contrary to the experimental results depicted in Figure 10. Possibly a trace amount of paramagnetic material is responsible for the unexpectedly short $T_1$ values measured at low temperatures.

**$^{2}H$ NMR of $ND_3$.** The $^{2}H$ powder spectrum of $d_3$PFF at 22 °C is shown in Figure 15A. A good simulation of the spectrum was obtained by summing three powder patterns. The three powder patterns were nearly axially symmetric. Their respective coupling constants and asymmetry parameters were 167 (±2) kHz, $\eta = 0.02$; 167 (±2) kHz, $\eta = 0.02$; and 129 (±2) kHz, $\eta = 0.05$. The established relationship between hydrogen-bond geometry

(41) Stark, R. E.; Haberkorn, R. A.; Griffin, R. G. *J. Chem. Phys.* **1978**, *65*, 1996.
(42) Schajor, W.; Post, H.; Grosescu, R.; Haeberlen, U.; Blockus, G. *J. Magn. Reson.* **1983**, *53*, 213.
(43) Halstead, T. K.; Speiss, H. W.; Haeberlen, U. *Mol. Phys.* **1976**, *31*, 1569.
(44) Sarkar, S. K.; Sullivan, C. E.; Torchia, D. A. *Biochemistry* **1985**, *24*, 2348.
(45) The principal axes for the chemical shift tensor are defined as $|\sigma_{zz}| \geq |\sigma_{xx}| \geq |\sigma_{yy}|$, $\eta = (\sigma_{yy} - \sigma_{xx})/\sigma_{zz}$, and $\sigma_{xx} + \sigma_{yy} + \sigma_{zz} = 0$ following ref 10. Note that this convention differs from that for the EFG trensor (ref 14 and Figure 1).

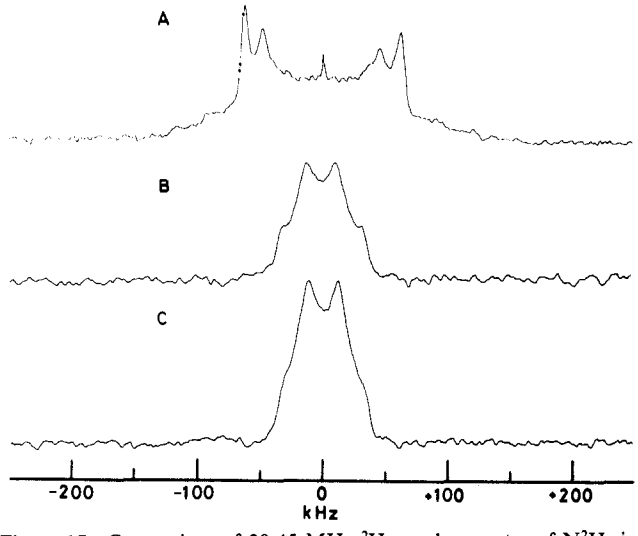


**Figure 15.** Comparison of 38.45-MHz $^2H$ powder spectra of $N^2H_3$ in *p*-fluoro-D,L-phenylalanine ($d_3$PFF) at two temperatures: (A) 22 °C; (B) and (C) 150 °C. Spectra were obtained by using a quadrupole echo pulse sequence with a 30-$\mu$s delay between 90° pulses in (A) and (B) and with 20-$\mu$s delay in (C). The 90° pulse width was 2.3 $\mu$s.

and the deuterium quadrupole coupling constant shows that the deuterium quadrupole coupling constant decreases as deuterium becomes involved in stronger hydrogen bonds.[46-50] The quadrupolar parameters obtained for $d_3$PFF at 22 °C were consistent with the hydrogen-bond N···O distances given in the X-ray structure.

The $^2H$ powder spectra showed that at 22 °C the reorientation of the $N^2H_3$ group is slow at the $^2H$ NMR time scale ($\omega_Q^{-1}$). Upon an increase in the temperature, the correlation time for reorientation of the $N^2H_3$ group decreased and a motionally averaged spectrum was observed (Figure 15B,C). However, an undistorted fast limit ($|\omega_Q\tau| \ll 1$) spectrum was not observed even at the highest temperature attained, 150 °C. This result was consistent with the hindered motion of $N^1H_3$ groups observed by Andrew and co-workers[38-40] in crystalline amino acids and is consistent with the strong hydrogen bonding observed here in $d_3$PFF. The motionally averaged powder spectrum was simulated by a single powder pattern having a quadrupole coupling constant of 48 kHz and $\eta = 0.37$. Within experimental error these values are in agreement with quadrupole parameters predicted by theory for three-site jumps of an $N^2H_3$ group having the static quadrupole parameters that were measured at 22 °C.

## Discussion

The most striking feature of the crystal structure of *p*-fluoro-D,L-phenylalanine is the arrangement of side-chain and backbone atoms into alternating layers that are normal to the *c* axis of the unit cell. The hydrophobic layer, composed of the phenyl side chains, is rather loosely packed. The ring carbon atoms are not in van der Waals contact with other atoms in the crystal and have large thermal factors. In contrast, the polar layer is composed of strongly hydrogen-bonded backbone atoms having much smaller thermal parameters. These structural features are consistent with (a) the NMR line shapes that show that the aromatic ring undergoes a rolling motion and 180° flips about the Cβ–Cl bond axis and (b) the deuterium quadrupole coupling constants of $ND_3$ observed at room temperature that indicate that the amine hydrogen atoms make strong hydrogen bonds.

The observation that the amplitude of the rolling motion in PFF increases as temperature increases indicates that the phenyl rings are less sterically hindered at high temperature, possibly because of crystal expansion. This hypothesis explains the curvature observed in the plot of $T_1$ vs. $1000/T$ (Figure 8), which indicates that the activation energy of the 180° ring flip decreases as temperature increases.

Examination of the PFF crystal structure shows that strong steric repulsions are encountered if one phenyl ring flips while its neighbors remain static. This fact and the relatively small value of the activation energy measured for the PFF ring flip (less than 20 kcal/mol) strongly suggests that the ring flip is a cooperative process in the PFF crystal, involving rolling motions of phenyl rings that are neighbors of the ring that flips.

A bilayer structure, similar to that observed for PFF, has been observed in the crystal structure of L-phenylalanine hydrochloride.[51] However, in the L-phenylalanine crystal structure all amino hydrogens are hydrogen bonded to the chlorine atom rather than the carbonyl oxygens, and the nitrogen is gauche with respect to the 1-carbon of the phenyl ring, rather than trans as found in the case of PFF. As a consequence of these differences in crystal structure, the detailed arrangement of the phenyl rings in the hydrophobic layer in the L-phenylalanine hydrochloride crystal differs from that in the PFF structure. These differences in the local environment of the phenyl rings in the two-crystal structures may be responsible for the difference in apparent activation energy for ring flips in crystalline L-phenylalanine hydrochloride, 17 kcal/mol,[52] and in crystalline PFF.

The phenyl-ring dynamics observed in crystalline PFF and L-phenylalanine hydrochloride contrast markedly with the ring dynamics observed in crystalline L-phenylalanine. When L-phenylalanine is crystallized from water, NMR spectra show that ca. 50% of the phenyl rings undergo rapid 180° flips ($\tau$ less than $10^{-9}$ s) at 20 °C.[2,5] The apparent activation energy measured for the phenyl-ring flip in crystalline L-phenylalanine, ca. 5 kcal/mol,[40,53] is significantly smaller than that found for crystalline PFF and L-phenylalanine hydrochloride. The structural basis for the relatively unhindered ring flips observed in crystalline L-phenylalanine is not understood because the crystal structure is not known. However, the evident propensity for L-phenylalanine molecules to form structures with loosely packed rings correlates with the difficulty in making mechanically stable single crystals of this compound.

The motionally averaged NMR spectra of crystalline L-phenylalanine cannot be accounted for by 180° ring flips alone. An analysis of $^{13}C$ NMR parameters has shown that the phenyl ring in crystalline L-phenylalanine, in addition to 180° flips, also executes a rolling motion (of the kind found herein for crystalline PFF) about the Cβ–Cl bond axis and a restricted isotropic motion.[54] We find no evidence of this latter type of motion in crystalline PFF, but this may be due to a more tightly packed ring environment in the case of PFF.

**Registry No.** *p*-Fluoro-DL-[2,3,5,6-$^2H_4$]phenylalanine, 101144-78-9; *p*-fluoro-DL-phenylalanine, 51-65-0.

(46) Soda, G.; Chiba, T. *J. Chem. Phys.* **1969**, *50*, 439.
(47) Hunt, M. J.; Mackay, A. L. *J. Magn. Reson.* **1974**, *15*, 402.
(48) Hunt, M. J.; Mackay, A. L. *J. Magn. Reson.* **1976**, *22*, 295.
(49) Butler, L. G.; Brown, T. L. *J. Am. Chem. Soc.* **1981**, *103*, 6541.
(50) Hiyama, Y. *Bunko Kenkyu* **1982**, *31*, 221.
(51) Al-Karaghouli, A. R.; Koetzle, T. F. *Acta Crystallogr., Sect. B: Struct. Crystallogr. Cryst. Chem.* **1975**, *B31*, 2461.
(52) Rice, D. M.; Gingrich, P.; Herzfeld, J.; Griffin, R. G. *Biophys. J.* **1982**, *37*, 145a.
(53) Kintanar, A. Ph.D. Thesis, University of Illinois, Urbana IL, 1984.
(54) Shaefer, J.; Stejskal, E. O.; Mackay, R. A.; Dixon, W. T. *J. Magn. Reson.* **1984**, *57*, 85.